Article type: Original Article

View metadata, citation and similar papers at core.ac.uk

Weathering regime in the Eastern Himalaya since the mid-Miocene: Indications from detrital geochemistry and clay mineralogy of the Kameng River Section, Arunachal Pradesh, India

Natalie Vögeli^{*,1}, Pascale Huyghe¹, Peter van der Beek¹, Yani Najman², Eduardo Garzanti³, Catherine Chauvel¹

¹ ISTerre, Université Grenoble Alpes, France

² Lancaster Environment Centre, Lancaster University, United Kingdom

³ Università Milano-Bicocca, Italy

*Corresponding author; ISTerre, Université Grenoble Alpes, 1381 Rue de la Piscine, 38041 Grenoble, Cedex 9, France ; natalievoegeli@gmail.com

Weathering regime in the Eastern Himalaya since the mid-Miocene: Indications from detrital geochemistry and clay mineralogy of the Kameng River Section, Arunachal Pradesh, India

Abstract

It is crucial to understand lateral differences in paleo-climate and weathering in order to fully understand the evolution of the Himalayan mountain belt. While many studies have focused on the western and central Himalaya, the eastern Himalaya remains poorly studied with regard to paleoclimate and past weathering history. Here we present a multi-proxy study on the Mio-Pliocene sedimentary foreland-basin section along the Kameng River in Arunachal Pradesh, northeast India, in order to obtain better insight in the weathering history of the eastern Himalaya. We analyzed a continuous sedimentary record over the last 13 Ma. Heavy-mineral and petrography data give insight into diagenesis and provenance, showing that the older part of the section is influenced by diagenesis and that sediments were not only deposited by a large Trans-Himalayan river and the palaeo-Kameng river, but also by smaller local tributaries. By taking into account changes in diagenesis and provenance, results of clay mineralogy and major element analysis show an overall increase in weathering intensity over time, with a remarkable change between ~10 and ~8 Ma.

This article has been accepted for publication and undergone full peer review but has not been through the copyediting, typesetting, pagination and proofreading process, which may lead to differences between this version and the Version of Record. Please cite this article as doi: 10.1111/bre.12242

1. Introduction

The Himalayan orogen has played an important role in the evolution of past climate (e.g. Raymo and Ruddiman, 1992; Molnar et al., 1993). The monsoonal climate, in turn, has a major influence on Himalayan erosion and relief patterns (Thiede et al., 2004; Bookhagen and Burbank, 2006; Clift et al., 2008). The Himalaya is therefore an excellent laboratory to investigate the links between climate, erosion and tectonics. Even though the evolution of the mountain belt is primarily driven by the India-Asia continent-continent collision, unravelling the past variations of monsoonal strength and weathering regimes is crucial to understanding the role of climate in the evolution of the mountain belt.

Chemical weathering and weathering fluxes to the ocean are a response to climate, tectonics and erosion (Galy and France-Lanord, 1999). Weathering fluxes and erosion rates in the Himalaya appear to have been relatively constant over the past 12 Ma, as recorded by sediments in the Bay of Bengal (Derry and France-Lanord, 1996; Galy et al., 2010). Lupker et al. (2012) showed that sediments are significantly weathered in the floodplain. However, past weathering regimes of the eastern Himalayan foreland basin sediments have never been properly constrained. Possible controls on these rates by monsoonal strength or tectonically controlled exhumation rates are not yet fully understood, although a possible relationship between Himalayan exhumation and monsoon intensification has been suggested (Clift et al., 2008).

Several sedimentary sections within the foreland basin of the Himalayan range, especially in the western and central Himalaya, have previously been dated and studied with the aim of determining hinterland exhumation rates, provenance and paleoclimate (Quade and Cerling, 1995; Huyghe et al., 2001; Ghosh et al., 2004; Sanyal et al., 2004; van der Beek et al., 2006 amongst others). However, the paleo-climate in the eastern Himalaya remains poorly studied.

We here present new data on the weathering history in the Eastern Himalaya by using whole-rock geochemistry and clay mineralogy from the Siwalik sedimentary record. Samples were collected from Miocene-Quaternary (13 to 1 Ma) foreland-basin sediments along the Kameng section in Arunachal Pradesh, northeastern India (Figure 1), which has been previously dated by magnetostratigraphy (Chirouze et al., 2012). To extract the weathering signal, it is crucial to also understand the provenance and diagenetic history of the sediments, in order to be able to deconvolve the signal. New heavy-mineral and petrography data are used as additional indicators for provenance and diagenesis and combined with existing data of Cina et al. (2009) and Chirouze et al. (2012, 2013). U-Pb ages of detrital zircons (Cina et al., 2009) as well as Nd and Hf bulk-rock isotopic

belt.

Brahmaputra sediments being de fission-track (AFT) ages (Chirouze sediments, which can be used as 2. Geological Setting 2.1. Himalayan Geology The formation of the Himalayan the Eurasian continental margins al., 2010; Hu et al., 2016) and sul 2000; Yin and Harrison, 2000). Th major lithotectonic units (Figure Himalayan Crystalline Series (HH These lithotectonic units are sep from north to south, the South T the Main Boundary Thrust (MBT) 2000; DeCelles et al., 2001). The granites, whereas the LHS are lar southernmost SH unit are the no were deposited in the Himalayan

data (Chirouze et al., 2013) suggest a change in provenance between 7 and 3 Ma, with paleo-Brahmaputra sediments being deposited in the Kameng river section during this period. Apatite fission-track (AFT) ages (Chirouze et al., 2013) show the maximum paleo-temperature in the sediments, which can be used as a first indicator for diagenesis.

The formation of the Himalayan mountain belt resulted from the collision between the Indian and the Eurasian continental margins, which began ca 60 to 50 Ma (e.g., Garzanti et al., 1987; Najman et al., 2010; Hu et al., 2016) and subsequently caused major crustal shortening and thickening (Hodges, 2000; Yin and Harrison, 2000). The Himalaya, south of the suture zone, can be divided into four major lithotectonic units (Figure 1), which are the Tethyan Sedimentary Series (TSS), the Higher Himalayan Crystalline Series (HHCS), the Lesser Himalayan Series (LHS) and the Sub-Himalayas (SH). These lithotectonic units are separated from each other by a series of north-dipping faults including, from north to south, the South Tibetan Detachment System (STDS), the Main Central Thrust (MCT), the Main Boundary Thrust (MBT) and the Main Frontal Thrust (MFT) (Le Fort, 1986; Yin and Harrison, 2000; DeCelles et al., 2001). The HHCS consist mainly of high-grade metasedimentary rocks and granites, whereas the LHS are largely Proterozoic low-grade metasedimentary rocks. The rocks of the southernmost SH unit are the non-metamorphosed clastic sediments of the Siwalik Group, which were deposited in the Himalayan foreland basin and are thrusted over the Indus-, Ganges- and Brahmaputra- alluvial plains along the MFT. North of the suture zone, the southern margin of the Asian plate is comprised of the Trans-Himalaya, which predominantly consists of Cretaceous-Paleogene Andean-type Gangdese batholiths (Wen et al., 2008). The suture zone itself, which is drained by the Yarlung-Brahmaputra River system, is marked by ophiolitic fragments amongst other lithologies (Hébert et al., 2012).

2.2. Foreland basin sediments – The Siwalik Group

The synorogenic sediments of the Siwalik Group form the foothills of the Himalaya along the entire mountain front from Pakistan to northeastern India. They represent the Neogene infill of the Himalayan foreland basin (DeCelles et al., 1998; Ojha et al., 2009; Chirouze et al., 2012). An overall coarsening- and thickening-upward trend is observed throughout the Siwalik Group, which is divided into the Lower, Middle and Upper Siwalik (LS, MS, US) sub-groups. The LS consist of alternating mudstone with some paleosols and fine- to medium-grained sandstone. The beds are a few meters thick. The LS is associated with a depositional environment of high-sinuosity streams. The MS consists of a stack of tens of meters thick medium- to coarse-grained mica-rich sandstone beds deposited by a large braided river system. The US contains tens of meters thick conglomerates with interlayers of sandstone and less commonly mudstone, and can be attributed to a gravelly braided river system (Nakayama and Ulak, 1999; Chirouze et al., 2013).

The Kameng River Section is located near the town of Bhalukpong in Arunachal Pradesh, northeastern India (Figure 1). The modern Kameng River drains the HHCS and the LHS before it flows through the Siwaliks and finally enters the floodplain where it flows into the Brahmaputra River. The Kameng River Section has been magnetostratigraphically dated by Chirouze et al. (2012) and spans from ca. 13 to 1 Ma. The exposed LS range from ca. 13 Ma to 10.5 Ma. The MS/US boundary was dated at 2.6 Ma (Chirouze et al, 2012). The Kameng River Section is approximately 6 km thick and is bounded to the south by the MFT, placing Siwalik rocks onto Quaternary sediments of the Brahmaputra plain (Burgess et al., 2012). The MBT separates the Siwaliks from the LHS in the north. Within the Kameng section, the Tippi Thrust places the LS over the US, therefore the younger part of the sequence, with MS and US exposure, is found in the footwall of the Tippi Thrust to the south, whereas the older part crops out in the structurally upper part of the section to the north (Figure 2). Detrital zircon U-Pb as well as bulk-rock Nd and Hf isotope data show that the Siwalik Group in the Kameng section was sourced from the HHCS and LHS by a paleo-Kameng River before 7 and after 3 Ma, while between 7 and 3 Ma the paleo-Brahmaputra brought in material sourced in the suture zone and Asian plate (Cina et al., 2009; Chirouze et al., 2013). Reset AFT ages can be used to constrain timing and burial depth (Chirouze et al., 2013). Sediments of the Kameng River section older than 8 Ma underwent burial diagenesis at temperatures above 110°C (Chirouze et al., 2013), the AFT annealing temperature (Donelick et al., 2005). The source-area exhumation rate in the Kameng river section appears to have remained fairly constant over the past 13 Ma, as determined from detrital zircon and apatite fission-track data (Chirouze et al., 2013).

3. Sampling and Methods

3.1. Sampling strategy

We sampled the Kameng River Section according to the lithological logs and magnetostratigraphic sampling points of Chirouze et al. (2012). Samples were collected in pairs of adjacent fine-(mud/siltstones) and coarse-grained (sandstones) sediment beds of the same age. To secure a continuous age record, 2-3 samples per Ma were collected. Additionally, modern river sand and mud

were sampled from the Kameng and Subansiri Rivers, which drain the Higher and Lesser Himalaya, and the Siang River, which additionally drains the suture zone and Asian plate. Previously sampled Yarlung river sediments were also analysed (cf. Figure 1).

3.2. Methods

3.2.1. Heavy Minerals and petrography

Heavy-mineral and sandstone petrography analyses were performed at the Department of Earth and Environmental Sciences at Università di Milano-Bicocca, using standard techniques as described in Garzanti and Andó (2007; see supplementary information for more details).

Sand/Sandstone petrography

A split aliquot of 16 Neogene sandstones and one modern sand sample were cut into standard thin sections, if necessary after impregnation with araldite, stained with alizarine red to distinguish dolomite and calcite, and analysed by counting 400 points under the petrographic microscope (Gazzi-Dickinson method; Ingersoll et al., 1984). Sand and sandstones are classified according to their main components (Q = quartz; F = feldspars; L = lithic fragments), considered only where QFL exceeds 10%. They are listed in order of abundance (e.g., in a feldspatho-quartzose sand Q > F > 10% QFL > L); an adjective reflecting the most common rock-fragment type may be added (e.g., metamorphiclastic).

Heavy minerals

Although bulk-sample analyses represent the only correct option for accurately estimating percentages of detrital minerals, the presence of detrital grains with great size differences in relatively poorly sorted alluvial sediments makes mounting and identification difficult (Mange and Maurer, 1992). Practical reasons thus exist to set lower and upper size limits to the analysed size-window, which in any case should be large enough to include most of the detrital population and thus to obtain a faithful characterization of the heavy-mineral suite (Garzanti et al., 2009). In this study we selected a very wide ($\geq 5 \phi$) size window for analysis (> 15 µm or 15-500 µm), and thus considered 85% of the bulk sediment, cutting only the extreme fine (12±7%) and coarse (3±3%) tails

of the size distribution. From a split aliquot of the chosen size-window separated by dry sieving, the dense fraction was separated by centrifuging in sodium polytungstate (density ~2900 kg/m³) and recovered by partial freezing with liquid nitrogen. From each sample, 200 to 280 transparent detrital minerals were analysed in grain mounts by point counting under the petrographic microscope, a technique that allows the true volume percentages of each mineralogical species to be obtained (Galehouse, 1971).

Heavy-mineral concentration was calculated as the volume percentage of total (HMC) and transparent (tHMC) heavy minerals (Garzanti and Andó, 2007). The complete results of petrographic and heavy-mineral analyses are provided in Appendix Table 1.

3.2.2. Clay minerals

Clay minerals were extracted from 21 selected, mostly fine-grained, samples. Samples were crushed to smaller pieces and diluted with MilliQ water. Carbonate and organic matter were removed by adding 20 ml buffer 1M acetic acid, with 50ml MilliQ and H_2O_2 , respectively, and heating the samples overnight. Samples were cleaned with MilliQ water after each removal. In order to separate the <2µm fraction, samples were diluted in MilliQ water and centrifuged for 8 min at 700 rpm, thereafter only the top 7 cm of the liquid, where the suspended load is situated, was pumped off. This procedure was repeated until a volume of 2 liters was achieved, in order to obtain sufficient clays for analysis (Moore and Reynolds, 1997). The fraction <2µm was stored in MilliQ water. Oriented aggregates were made on glass slides. X-ray diffractograms were carried out on air-dried and ethylene-glycol treated samples on a Siemens Bruker D8 Advance X-Ray Diffractometer at ISTerre, Université Grenoble-Alpes.

A semi-quantitative peak analysis on the XRD patterns was undertaken in order to characterise the clay-mineral distribution. This method is based on the XRD peak height of the different clay minerals by adding them up to 100% (Capet et al., 1990), allowing a relative percentage of different clay minerals with a relative error of approximately 5% to be obtained (Holtzappel, 1985). In this paper, authigenic clays, such as smectites, which are produced under enhanced weathering conditions (Hillier, 1995) are used to characterise the intensity of weathering.

With increasing burial and very low-grade metamorphism, smectites and illite–smectite mixed-layers re-crystallize and progressively transform into illites and finally into muscovite (Lanson et al, 1996). These transformations, very complex in detail, lead to a progressive decrease in the width of the 10 Å peak as measured on X-ray diffractogram. Illite crystallinity, also known as Kübler Index (KI), is the full width at half maximum (FWHM) of the 10 Å peak on the air-dried X-ray diffractogram (Kübler

and Goy-Eggenberger, 2001). Therefore, low KI values correspond to well-crystallized minerals, whereas high KI values indicate poorly crystallized minerals. The KI measurement is thus a statistical means to discriminate low-grade metamorphic (detrital) and diagenetic illites in sedimentary rocks: increasing KI indicates stronger diagenetic overprint. We measured the FWHM on air-dried and ethylene-glycol treated samples. The illite peak on the air-dried samples takes into account smectite-illite mixed layers. The KI measurements allow us to establish three subdivisions within the low-grade metamorphism field: diagenesis, anchizone and epizone (Warr and Rice, 1994).

3.2.3. Major elements

Pairs of fine- and coarse-grained samples were ground to a powder with an agate mortar. Loss of ignition (LOI) was determined by weight loss after heating for an hour at 1000 °C. Major element concentrations were determined after dissolution of 50-70 mg of powder in a mixture of HF and HNO_3 heated for about 72 h at 90 °C. The solution was then treated with boric acid to neutralize the HF and with H_2O_2 to dissolve organic matter, and further diluted with MilliQ water. Analyses were performed using a Varian 720-ES inductively coupled plasma atomic emission spectrometer (ICP-AES) at ISTerre, Université Grenoble-Alpes, following the method of Chauvel et al. (2011). The accuracy of the measurements is evaluated at ~3% by comparing the concentrations measured on international reference material, run as unknown, with the reference values (Appendix Table 2). Hydration (H_2O^+) of selected samples was measured at the SARM, CNRS, CRPG in Nancy, France with the Karl Fischer titration method (Fischer, 1935).

Classical weathering proxies such as the Chemical Index of Alteration (CIA; Nesbitt and Young, 1982) or the Weathering Index of Parker (WIP; Parker, 1970) are strongly dependent on grainsize and provenance (cf. Lupker et al., 2012, 2013 and references therein), as well as by diagenesis, e.g., precipitation of calcite or dolomite in the cement. Therefore, we illustrate the degree of chemical weathering of the sedimentary rocks by using ratios of mobile to immobile elements, such as K/Si, H_2O^+/Si and K/AI (Lupker et al., 2013). Sediment hydration, H_2O^+ , is a proxy for chemical weathering that traces mineral hydrolysis and secondary neo-formations (Lupker et al., 2012). K/Si and H_2O^+/Si are dominantly controlled by the grain size of sediments in modern rivers, and secondarily by weathering. K/Si and H_2O^+/Si ratios were therefore normalized to a common average Al/Si composition of 0.22, with a regression line through a coarse-grained end member and the sample (Appendix Table 1 and Lupker et al., 2013). Resulting normalised values of K/Si* and $H_2O^+/Si*$ are used together with the K/AI ratio to quantitatively track weathering trends through time.

4. Results

4.1. Heavy minerals and petrography

Compositions of Siwalik sandstones are shown in Figure 3. The oldest sample (KM13-5, 13 Ma), which was collected in proximity of the Tippi Thrust, is a virtually pure quartzarenite with very low-rank metasedimentary rock fragments and an extremely poor, zircon-dominated heavy-mineral assemblage. Detrital modes contrast with those of modern Kameng sand.

The overlying sandstone samples (13 to 8 Ma) in the hanging wall of the Tippi Thrust range from feldspatho-quartzose to litho-feldspatho-quartzose metamorphiclastic with approximately equal amounts of plagioclase and K-feldspar, more abundant biotite than muscovite, and mainly schist, gneiss, metasandstone, slate/phyllite and granitoid rock fragments. A few dolostone rock fragments appear upward. Heavy-mineral assemblages are very poor and garnet-dominated with tourmaline, zircon, apatite and rutile.

The ZTR index (sum of zircon, tourmaline and rutile over total transparent heavy minerals), which constitutes an indicator of mineralogical stability (Hubert, 1962), lies between ~20 and 50 (with an outlier at 13 Ma) through the 13-8 Ma LS to MS succession exposed in the hanging wall of the Tippi Thrust (Figure 4). Transparent heavy-mineral percentages are invariably very poor with dominant garnet, epidote only sporadically recorded, and amphibole, staurolite, kyanite and sillimanite never recorded.

By contrast, in the MS and US section exposed in the footwall of the Tippi Thrust (samples aged < 8 Ma), excepting samples KM13-2 (8.3 Ma) and KM13-19c (2 Ma), ZTR is mostly less than one. Heavymineral assemblages range from moderately poor to rich and mainly include amphibole, garnet and epidote, with minor kyanite, chloritoid and staurolite. Amphibole and epidote are invariably abundant, whereas fibrolitic sillimanite becomes common at 3-4 Ma. Sandstone samples in the central part of the MS (8-3 Ma) are litho-feldspatho-quartzose metamorphiclastic rocks with approximately equal amounts of plagioclase and K-feldspar, more abundant biotite than muscovite, and mainly schist, gneiss, metasandstone, slate/phyllite, granitoid, volcanic, metavolcanic and siltstone/sandstone rock fragments. The composition of this 8-3 Ma interval is comparable to that of the modern Kameng and Brahmaputra rivers, with the exception of two samples at 8.3 and 2 Ma (Figure 3).Intercalated in both the lowermost (KM13-2, 8.3 Ma) MS and lowermost (KM13-19, 2 Ma) US are feldspatho-quartzose to quartzose sandstones with more abundant K-feldspar than plagioclase, minor metamorphic rock fragments and very poor heavy-mineral assemblages including abundant (or even dominated by) zircon and tourmaline.

The youngest sandstone sample (KM13-20, ~0.8Ma) is a litho-feldspatho-quartzose with more abundant K-feldspar than plagioclase, more abundant biotite than muscovite and mainly low-rank metamorphic rock fragments. The moderately poor heavy-mineral assemblage includes garnet, amphibole, epidote, tourmaline, kyanite and mainly fibrous sillimanite. Composition is broadly similar to modern Kameng sand.

Modern Kameng sand is litho-feldspatho-quartzose metamorphiclastic, with approximately equal amounts of plagioclase and K-feldspar, more abundant biotite than muscovite, and mainly gneiss, schist, granitoid, shale and metasandstone rock fragments. Moderately rich heavy-mineral assemblages include abundant hornblende, garnet, subordinate epidote, minor tourmaline and fibrous and prismatic sillimanite.

4.2. Clay mineralogy

Clay minerals in the <2µm fraction of clayey beds in the Siwalik Group consist mainly of illite, chlorite, smectite and kaolinite (Figure 5). The clay-mineral assemblage varies with time and depth within the Kameng section. The oldest part of the section, from 13 to 8 Ma, is dominated by illiteand chlorite-rich assemblages (illite+chlorite/∑clays > 0.5). The part of the section dated between 8 and 3 Ma is dominated by a higher smectite content of around 50 %. From 3 to 1 Ma, around the boundary of the MS and US, kaolinite is the most abundant clay mineral, whereas smectite is virtually absent. Strata younger than 1 Ma are again characterized by higher smectite contents. The oldest sample (13 Ma) differs from the rest and has an unusually high smectite content for its depth. Another outlier is the sample at 4 Ma, a sandstone with extremely low clay content. XRD peaks are small for this sample, making precise semi-quantitative analysis difficult; it therefore should be interpreted with caution.

Illite crystallinity (KI) varies from 0.11 to 0.53 $\Delta^{\circ}2\theta$ on the ethylene-glycol treated samples and 0.11 to 0.60 $\Delta^{\circ}2\theta$ on air-dried samples. There is no clear trend throughout the section (Figure 5), with most of the values lying between 0.1 and 0.3 $\Delta^{\circ}2\theta$ on EG samples; only two values are > 0.4 $\Delta^{\circ}2\theta$. Samples with KI < 0.3 $\Delta^{\circ}2\theta$ are dominated by well-crystallized minerals with crystallinity similar to muscovites from the HHCS (Huyghe et al., 2011). Samples KM13-1 (8.6 Ma) and KM13-9 (2 Ma), with KI > 0.4 $\Delta^{\circ}2\theta$), in contrast, contain poorly crystallized minerals, such as diagenetic illite and illite-smectite mixed layers.

Clay-mineral assemblages from modern eastern Himalayan rivers (Yarlung, Siang, Subansiri and Kameng) are shown in Figure 6. They are dominated by illite and chlorite (illite+chlorite/∑clays > 0.7), except the uppermost sample of the Yarlung River, which has almost 50 % smectite. Overall,

the proportion of illite and chlorite increases downstream. Muds of the Yarlung upstream of the Eastern Syntaxis have a higher smectite content, compared to downstream. Himalayan tributaries to the Brahmaputra such as the Subansiri and the Kameng have an illite content of up to ~90% (illite+chlorite/ Σ clays >0.8).

4.3. Major elements and H₂O⁺

Major-element concentrations were measured on pairs of coarse- and fine-grained samples of similar age, where possible (Appendix Table 1). The difference between coarse- and fine-grained samples is well reflected in the major-element composition, as shown in Figure 7: sandstones generally have higher SiO₂, whereas finer sediments such as mudstones have a higher K₂O, Al₂O₃ and H_2O^+ . The ratio of the immobile elements Al₂O₃/SiO₂ is thus a direct reflection of grain size (Lupker et al., 2012). The modern Kameng muds have a relatively high SiO₂ concentration of approximately 79 wt%.

Differences in grain size are also obvious when Al/Si is plotted against K/Si (Figure 8), with much lower Al/Si and K/Si ratios for coarse-grained sediments due to higher proportions of quartz grains in the coarse fraction. Lupker et al. (2013) also used this diagram to highlight the degree of chemical weathering: unaltered protolith produces sediment with high K/Si at a given Al/Si while weathering removes mobile elements such as K and lowers the K/Si ratio (Figure 8). We calculated the 95% confidence interval of the regression for each of the three groups within the Siwaliks (LS, MS and US) and found that regression lines had significantly different slopes. Sediments of the LS define a steep slope and fall next to the data reported by Lupker et al (2013) for the Himalayan tributaries; by contrast, the MS and US samples define flatter slopes in Figure 8 and plot close to the Brahmaputra samples of Lupker et al. (2013). The relatively limited number of analysed samples from both the MS and the US renders the difference between these two groups statistically insignificant.

Normalized ratios allow for the comparison of chemical compositions of samples with different grain sizes (e.g. sandstone and mudstone). Normalized ratios K/Si* and H_2O^+/Si^* versus age are shown in Figure 9. K/Si* and K/Al show similar trends with rather constant and high ratios between 13 and 10 Ma, followed by a period of lower values, which indicates more weathered rocks. The lack of fine-grained sediments between 8 and 3 Ma renders the interpretation of the trend in this part of the section difficult. In the period from 4-1 Ma ratios are widely spread, with a significant difference between coarse- and fine-grained rocks. Modern river K/Si* and K/Al values are again higher.

5. Discussion

Extracting weathering history from the sedimentary record requires understanding the provenance of the sediments and degree of diagenesis that they have been subjected to, in order to be able to deconvolve the chemical and mineralogical signal. In the following, we therefore first review existing and our new data in terms of provenance and diagenesis, before discussing the weathering signal.

5.1. Provenance evolution of the Kameng sediments

Previous studies have shown changes in provenance in the Kameng section through time (Cina et al., 2009; Chirouze et al., 2013). εNd variations indicate paleo-Brahmaputra provenance between 7 and 3 Ma (Chirouze et al., 2013), with less negative εNd values of around -13, characteristic for the modern Brahmaputra (Singh and France-Lanord, 2002), during this time interval compared to values between -15 and -18, close to modern Kameng sand, in samples above and below this interval. This change in provenance is supported by U-Pb zircon ages (Cina et al., 2009), with ages <200 Ma including a major cluster between 40-60 Ma, being present in the MS, but not in the LS. Such ages are typical of zircons derived from the Cretaceous-Paleogene Transhimalayan Gangdese batholith (Cina et al., 2009), which forms a major part of the Yarlung-Brahmaputra drainage (Figure 1).

Modern Kameng sand indicates provenance largely from the HHCS, with significant contribution from the LHS, revealed by relatively low metamorphic indices, and probably some recycling of Siwalik molasse units accreted at the front of the orogen (Garzanti et al., 2004). Siwalik sandstones in the Kameng section display several significant mineralogical changes, traced by variations of petrographic and mineralogical indices (Figure 3). Sudden changes, often represented by a single sample (e.g., KM13-2 and KM13-19c), are ascribed to sediments deposited by tributaries of limited length, draining the Himalayan foothills (Garzanti and Andó, 2007), intercalated with trunk-river deposits as a consequence of lateral channel shifts. Deposits of small tributaries can be associated with recycling of Siwalik molasse or erosion of quartzites, abundant in the LHS of Arunachal Pradesh (Yin et al., 2006). All other sandstone samples, i.e. KM13-26c to KM13-1 (13-8 Ma), KM13-30c to KM13-28c (7-3 Ma) and KM13-20c (~0.8Ma) represent deposition by a major trunk river, i.e. either a paleo-Kameng or a paleo-Brahmaputra River (Figure 3).

A more varied lithic population characterizes sandstones between 7 and 3 Ma, where volcanic, metavolcanic and metabasite rock fragments are more frequently recorded, associated with sedimentary to low-rank meta-sedimentary lithic fragments. These rock fragments could be derived from north of the Higher Himalaya, which would be consistent with a contribution from Suture Zone and Transhimalayan units and possible deposition by a paleo-Brahmaputra longitudinal trunk river (Chirouze et al., 2013), as evidenced from Sm-Nd bulk geochemistry and U-Pb detrital zircon ages, as detailed above. Staurolite, kyanite and sillimanite appear and tend to become more abundant upward, documenting provenance from amphibolite-facies HHCS granitoid gneisses and schists since ~8 Ma. Nevertheless, biotite is the predominant detrital mica since 12 Ma, suggesting provenance from amphibolite-facies rocks of the HHCS.

Clay-mineral assemblages represent a mixture of detrital and authigenic clays (Hillier, 1995; Huyghe et al., 2005). Diagenetic transformations occurring during burial further complicate the provenance signal. An increased smectite content is observed in the Kameng section between 7 and 3 Ma, during the time interval in which we infer deposition by a paleo-Brahmaputra River. Modern rivers in the eastern Himalaya (Kameng, Subansiri, Siang) have relatively poor smectite content, in contrast to the uppermost Yarlung River sample. The higher smectite content in this Yarlung sample could be related to weathering of mafic and ultramafic rocks found in the suture zone. However, the smectite component is reduced in the Siang River downstream, due to input from Himalayan rivers draining catchments with lower smectite content and/or rapid erosion of the Namche Barwa syntaxis. We therefore would expect paleo-Brahmaputra deposits to have lower smectite content compared to the Yarlung, assuming that rapid erosion of the Namche Barwa syntaxis was active at the given time, and similar smectite content to rivers such as the Kameng, draining the southern Himalayan slopes only. We therefore do not correlate this variation in clay mineralogy to provenance variations in the Kameng section, and rather suggest that the dominance of smectite in the clay mineral assemblage is related to a change in diagenesis or weathering regime.

5.2. Diagenesis

Partially reset AFT ages below ~4000 m of estimated burial depth in the Kameng section (Chirouze et al., 2013) are a clear indicator that sediments were heated to at least 60 °C, the temperature above which partial AFT annealing starts (e.g., Tagami and O'Sullivan, 2005). This trend is confirmed by the ZTR index showing diagenetic dissolution of less stable heavy minerals, which is detected from a depth of about 3500 m corresponding to a depositional age of ~8 Ma (Figures 2 & 4). Less stable detrital minerals may undergo extensive and even complete intrastratal dissolution during burial diagenesis, leaving behind a residual assemblage that may differ substantially from the original depositional suite. Mineralogical trends observed up-section, therefore, are typically the result of selective diagenetic control superposed on provenance and paleo-drainage changes, which can render the interpretation equivocal. Grains in the footwall of the Tippi Thrust, younger than 8 Ma, show little evidence of corrosion and have significantly lower ZTR indices (Figure 3). The influence of diagenesis therefore appears negligible in this age bracket.

Illite crystallinity or Kübler Index (KI) (Kübler and Jaboyedoff, 2000; Kübler and Goy-Eggenberger, 2001) allows the detection of illitisation of smectites that starts at temperatures of about 70-95°C (Dunoyer De Segonzac, 1970). AFT data from the central part of the Siwalik foreland basin suggest that these temperatures were reached at depths of approximately 1800-2000 m (van der Beek et al., 2006). However, besides the increase of temperature with depth, many other factors (geochemical peculiarities of different sequences, kinetics, fluids etc.) may influence the progress of this reaction, complicating attempts to use it as a geothermometer (Hillier, 1995). Deterioration of illite crystallinity, hence increasing KI, is not observed within the Kameng section, whereas it was shown to take place below 2100 m depth in the Karnali section (Huyghe et al., 2005). This result suggests that (1) the clay fraction of the Kameng samples mainly contains inherited illites that were affected by metamorphism in their source area and (2) not all of the smectites in this part of the Siwalik foreland basin have been illitised. Nonetheless, two samples (at 2 and 9 Ma) display illites with poor crystallinity. The 2-Ma sample is from a stratigraphic depth of ~1000 m where smectite is unlikely to be illitised; however, this sample also shows anomalous provenance from the outer LHS and we suggest that the low-crystallinity illites were formed in the source rock. In the 9 Ma sample, from a stratigraphic depth of ~4000 m, partial illitisation is possible.

Diagenetic reactions and post-depositional weathering would lead to a loss of mobile elements (recorded as increasing weathering indices) down-section (Lupker et al., 2013). As mobile major elements do not show a decrease with depth and time, we can assume that major-element concentrations are not strongly affected by diagenesis (Figure 9). Only sample KM13-5 at 13 Ma, which is located in proximity to the Tippi Thrust, shows major depletion in mobile elements, as well as an abnormal clay and heavy-mineral composition. The anomalous features of this sample are likely due to fluid circulation within the damage zone of the Tippi Thrust, leaving behind pure quartzite and leaching mobile major elements, as well as forming secondary smectite.

5.3. Weathering regime in the Eastern Himalaya since 13 Ma

Ratios of mobile to immobile major elements have been shown to efficiently track weathering of sediments (Lupker et al., 2012, 2013). Here, we use the ratio of K/Al to show trends in weathering of sediments (Figures 8 & 9). If we consider that weathered rocks experience fluid-rock interactions, then a loss of potassium reflects stronger weathering. In order to rule out the influence of grain size, normalized ratios K/Si* and H_2O^+/Si^* are used to compare sediments with different grain sizes (Bouchez et al., 2012; Lupker et al., 2012, 2013). Especially the K/Si* and the K/Al ratios show an increase in weathering starting around 10 Ma, reaching a maximum at ~8 Ma, and remaining high afterwards. This timing corresponds well with the smectite-rich period, also starting at ~8 Ma. Thus,

two independent proxies show a change towards increased weathering between 10 and 8 Ma. The fact that smectite is absent in the modern Transhimalayan rivers suggests that smectite in the Kameng section was formed secondarily by weathering, rather than being brought in with the paleo-Brahmaputra at that time. Smectite-kaolinite rich assemblages persist in the Upper Siwaliks. The same change in clay mineralogy has been observed in other Siwalik sections, such as the Karnali and Surai Khola in western Nepal (Huyghe et al., 2005), as well as in the distal Bay of Bengal (France-Lanord et al., 1993; Galy et al., 1996) and was ascribed to environmental change. However, new results from IODP Expedition 354 in the Bengal Fan do not show a similar change in clay mineralogy (France-Lanord et al., 2015).

Rocks younger than 3.5 Ma, mostly US sediments, show greater variations of K/Si^{*}, H_2O^+/Si^* and K/Al ratios, which vary from indicating strongly weathered to less weathered rocks. A strong weathering signal in US sediments could potentially be biased by recycled Siwalik molasse. US sediments might thus have partly experienced weathering twice, once before and once after they were recycled. Modern river sediments, in contrast, are less weathered than the US.

A trend towards stronger weathering can be observed from the Lower to the Upper Siwaliks (Figure 8). Confidence levels of the regression lines show a clear separation of the LS, which are less weathered, from the MS and US, which overlap but are clearly more weathered than the LS. Rocks in proximity to the Tippi Thrust differ strongly from all other data points (and are not taken into account for the regression lines), showing extreme depletion of potassium. Overall a strengthening in the degree of weathering is observed upsection, but it remains hard to quantify the amount of change.

The location of deposition within the basin should be taken into account when interpreting trends in weathering proxy data from the sedimentary record; since weathering is focused in the floodplain, detritus in modern mountain-front rivers is typically less weathered compared to detritus in rivers of the floodplain (Lupker et al., 2012). The LS were deposited in the floodplain, whereas MS and US were deposited more proximal to the mountain front. We would therefore expect LS to be more weathered than younger sediments, if the signal was dominantly the result of position with respect to the floodplain. This is not the case, however; both the trend to increased weathering through time, and the significant shift at 8 Ma are not consistent with a hypothesis whereby the trend is due to position within the foreland basin.

Quade and Cerling (1995) have suggested an intensification of the Indian Summer Monsoon at 7 Ma, from stable carbon-isotope records in paleosols from Pakistan and Nepal. Sanyal et al. (2010) defined several periods of strong monsoon intensity at 11, 6 and 3 Ma, by looking at isotope ratios of

pedogenic clay and carbonates of the Siwaliks in northwestern India. Clift et al. (2008) suggest a strong monsoon from 16 to 10 Ma with a gradual weakening afterwards between 10 and 3 Ma. Sediment accumulation rates and grain size in the distal Bengal fan decrease between 7 and 1 Ma (France-Lanord et al., 1993). Our data shows decreasing K/Al, also seen in the Bengal Fan by Clift et al. (2008). Together with enhanced smectite abundance, this suggests a stronger weathering regime starting at ~8 Ma, which could be linked to a more seasonal climate. An overall increase in weathering is observed in the Kameng section. US sediments younger than 3.5 Ma might partly be recycled, potentially biasing the weathering signal, but nevertheless seem more weathered than those from the LS. These rather subtle changes in weathering are probably linked to changes in seasonality as well as to local changes in climate and precipitation patterns. Less intense weathering in the older part of the section could be linked to higher runoff and faster sediment transport, hence less residence time in the floodplain, which might indicate a less seasonal climate. Such a scenario would be similar to what is observed in the western Himalaya, even though the eastern Himalayan sedimentary record does not show a trend to stronger seasonality as clear as the west (Vögeli et al., 2015).

Several authors have suggested potential feedback links between formation of the main Himalayan thrusts (MFT, MBT, MCT), climate, and erosion and weathering rates (e.g., Clift et al., 2008; Armstrong and Allen, 2010). However, thrust activation remains hard to date and poorly studied in the eastern Himalaya. Robinson et al. (2003) suggest onset of the MCT in the Early Miocene, before deposition of the Kameng sediments. The onset of movement along the MBT in the eastern Himalaya is not well constrained, but as the MBT thrusts the LHS over the 8-Ma MS rocks, the onset of MBT motion must post-date 8 Ma. The onset of movement along the local Tippi Thrust and the MFT is dated at around 1 Ma (Chirouze et al., 2013). There is no obvious correlation of activation of these thrusts with changes in weathering. The source-area exhumation rates recorded by the Kameng sediments are relatively constant (Chirouze et al., 2013); therefore, the change in weathering between ~10-8 Ma is likely climatically controlled rather than being strongly influenced by tectonics. In particular, weathering appears to have been influenced by variations in moisture transport from the Bay of Bengal, even though these were not sufficient to trigger a change in vegetation in the eastern Himalaya as recorded by carbon stable-isotope data (Vögeli et al., 2015).

6. Conclusion

The Himalayan record of foreland basin sediments holds valuable information on past weathering regimes. Provenance and diagenesis can strongly influence the sedimentary record; nevertheless by taking variations in provenance, diagenesis and grain size into account, weathering signals can be extracted from the geochemistry and mineralogy of the foreland-basin sediments.

Heavy-mineral assemblages and petrography document repeated provenance changes, with deposits of local tributaries episodically interbedded with trunk-river deposits chiefly derived from the LHS and HHCS, similar to the modern Kameng and Brahmaputra. Diagenetic dissolution of less stable minerals is extensive in the lower part of the section. Although the mineralogical composition of the sediments appears affected by diagenesis, its influence on major-element composition and clay mineralogy appears minimal.

Changes in weathering are subtle, but they exist. There is an overall increase in weathering intensity from the Lower Siwaliks to the Middle and Upper Siwaliks. Clay-mineral assemblages and majorelement compositions independently indicate an increase in weathering intensity between ~10 and 8 Ma, and a regime of enhanced weathering since ~8 Ma. Another change at ~3.5 Ma is probably linked to the onset of Siwalik recycling, possibly in conjunction with a wetter climate. Changes in K/Al and K/Si*, together with a high smectite abundance since 8 Ma, do not correlate with the changes in provenance; we therefore interpret them as an enhanced weathering signal, caused by a more seasonal and overall drier climate in the eastern Himalaya since this time. As exhumation and accumulation rates stay more or less constant over the last 13 Myr, we suggest that the change in weathering environment originates from climatic rather than tectonic variations. The eastern part of the Himalaya is located in proximity to the main moisture source in the Bay of Bengal. The subtle change in the weathering regime indicates that the climate of the eastern Himalaya has stayed rather constant over the last 13 Myr, with a change towards more seasonality between ~10 and 8 Ma and generally becoming more seasonal and possibly overall drier. Such a change would result in less runoff and a longer residence time of sediments in the floodplain, and therefore an increase in weathering intensity. The impact on vegetation and other environmental parameters remains to be discussed and investigated with different methods.

The Siwalik sedimentary record bears important proximal information on paleo-climate. Compared to the marine record, foreland-basin sediments constitute a more proximal source, limiting potential bias of the signal by transport far into the ocean. Multiproxy analyses are crucial for such studies. Clay mineralogy in combination with major-element analysis can give new insights into past weathering regimes, even though quantification of weathering rates remains challenging.

Acknowledgements

We thank Gwladys Govin and Lorenzo Gemignani for field assistance, and Christian France-Lanord for inputs and discussions as well as providing additional clay and major-element data. Kattu is thanked for logistics and organization during fieldwork. We acknowledge financial support from Marie Curie Initial Training Network iTECC, funded by the EU REA under the FP7 implementation of the Marie Curie Action, under grant agreement # 316966. Comments by Peter Clift, Thierry Adatte and one anonymous reviewer helped to improve the manuscript.

No conflict of interest declared

References

- Armstrong, H.A., and Allen, M.B., 2010, Shifts in the Intertropical Convergence Zone, Himalayan exhumation, and late Cenozoic climate: Geology, v. 39, no. 1, p. 11–14, doi: 10.1130/G31005.1.
- Bookhagen, B., and Burbank, D. W., 2006, Topography, relief, and TRMM-derived rainfall variations along the Himalaya: Geophysical Research Letters, v. 33, no. 8, L08405.
- Bouchez, J., Gaillardet, J., Lupker, M., Louvat, P., France-Lanord, C., Maurice, L., Armijos, E., and Moquet, J.-S., 2012, Floodplains of large rivers: Weathering reactors or simple silos?: Chemical Geology, v. 332–333, p. 166-184.
- Burgess, P. W., Yin, A., Dubey, C. S., Shen, Z.-K., and Kelty, T. K., 2012, Holocene shortening across the Main Frontal Thrust zone in the eastern Himalaya: Earth and Planetary Science Letters, v. 357–358, p. 152-167.
- Capet, X., Chamley, H., Beck, C., and Holtzappel, T., 1990, Clay mineralogy of ODP sites 671 and 672, Barbados Ridge Accretionary Complex and Atlantic Abyssal Plain: palaeoenvironmental and diagenetic implications.: In: Proceedings of the Ocean Drilling Program, Scientifc Results, Vol. 110 (Ed. by A.Mascle, J.C. Moore & E. Taulor, et al.). Ocean Drilling Program, College Station,TX, p. 85-96.
- Chauvel, C., Bureau, S., and Poggi, C., 2011, Comprehensive Chemical and Isotopic Analyses of Basalt and Sediment Reference Materials: Geostandards and Geoanalytical Research, v. 35, no. 1, p. 125-143.
- Chirouze, F., Dupont-Nivet, G., Huyghe, P., van der Beek, P., Chakraborti, T., Bernet, M., and Erens,
 V., 2012, Magnetostratigraphy of the Neogene Siwalik Group in the far eastern Himalaya:
 Kameng section, Arunachal Pradesh, India: Journal of Asian Earth Sciences, v. 44, p. 117-135.
- Chirouze, F., Huyghe, P., van der Beek, P., Chauvel, C., Chakraborty, T., Dupont-Nivet, G., and Bernet, M., 2013, Tectonics, exhumation, and drainage evolution of the eastern Himalaya since 13
 Ma from detrital geochemistry and thermochronology, Kameng River Section, Arunachal Pradesh: Geological Society of America Bulletin, v. 125, no. 3-4, p. 523-538.
- Cina, S. E., Yin, A., Grove, M., Dubey, C. S., Shukla, D. P., Lovera, O. M., Kelty, T. K., Gehrels, G. E., and Foster, D. A., 2009, Gangdese arc detritus within the eastern Himalayan Neogene foreland basin: Implications for the Neogene evolution of the Yalu–Brahmaputra River system: Earth and Planetary Science Letters, v. 285, no. 1–2, p. 150-162.
- Clift, P. D., Hodges, K. V., Heslop, D., Hannigan, R., Van Long, H., and Calves, G., 2008, Correlation of Himalayan exhumation rates and Asian monsoon intensity: Nature Geosci, v. 1, no. 12, p.

875-880.

- DeCelles, P. G., Gehrels, G. E., Quade, J., Ojha, T. P., Kapp, P. A., and Upreti, B. N., 1998, Neogene foreland basin deposits, erosional unroofing, and the kinematic history of the Himalayan fold-thrust belt, western Nepal: Geological Society of America Bulletin, v. 110, no. 1, p. 2-21.
- DeCelles, P. G., Robinson, D. M., Quade, J., Ojha, T. P., Garzione, C. N., Copeland, P., and Upreti, B.
 N., 2001, Stratigraphy, structure, and tectonic evolution of the Himalayan fold-thrust belt in western Nepal: Tectonics, v. 20, no. 4, p. 487-509.
- Derry, L. A., and France-Lanord, C., 1996, Neogene Himalayan weathering history and river87Sr86Sr: impact on the marine Sr record: Earth and Planetary Science Letters, v. 142, no. 1–2, p. 59-74.
- Donelick, R. A., O'Sullivan, P. B., and Ketcham, R. A., 2005, Apatite Fission-Track Analysis: Reviews in Mineralogy and Geochemistry, v. 58, no. 1, p. 49-94. Dunoyer De Segonzac, G., 1970, The transformation of clay minerals during diagenesis and low-grade metamorphism: A review.: Sedimentology, v. 15, no. 3-4, p. 281-346.
- Fischer, K., 1935, Neues Verfahren zur maßanalytischen Bestimmung des Wassergehaltes von Flüssigkeiten und festen Körpern: Angewandte Chemie, v. 48, no. 26, p. 394-396.
- France-Lanord, C., Derry, L., and Michard, A., 1993, Evolution of the Himalaya since Miocene time: isotopic and sedimentological evidence from the Bengal Fan: Geological Society, London, Special Publications, v. 74, no. 1, p. 603-621.
- France-Lanord, C., Spiess, V., Klaus, A., and the Expedition 354 Scientists, 2015, Bengal Fan: Neogene and late Paleogene record of Himalayan orogeny and climate: a transect across the Middle Bengal Fan.: International Ocean Discovery Program Preliminary Report, 354.
- Galehouse, J. S., 1971, Point Counting: In: Carver, R.E. (Ed.), Procedures in sedimentary petrology. Wiley, New York, p. 385-407.
- Galy, A., and France-Lanord, C., 1999, Weathering processes in the Ganges–Brahmaputra basin and the riverine alkalinity budget: Chemical Geology, v. 159, no. 1–4, p. 31-60.
- Galy, A., France-Lanord, C., and Derry, L. A., 1996, The Late Oligocene-Early Miocene Himalayan belt Constraints deduced from isotopic compositions of Early Miocene turbidites in the Bengal Fan: Tectonophysics, v. 260, no. 1–3, p. 109-118.
- Galy, V., France-Lanord, C., Peucker-Ehrenbrink, B., and Huyghe, P., 2010, Sr–Nd–Os evidence for a stable erosion regime in the Himalaya during the past 12 Myr: Earth and Planetary Science Letters, v. 290, no. 3–4, p. 474-480.
- Garzanti, E., Baud, A., and Mascle, G., 1987, Sedimentary record of the northward flight of India and its collision with Eurasia (Ladakh Himalaya, India): Geodinamica Acta, v. 1, p. 297-312.
- Garzanti, E., and Andó, S., 2007, Heavy-mineral concentration in modern sands: implications for provenance interpretation.: In: Mange, M.A., Wright, D.T. (Eds.), Heavy Minerals in Use. Elsevier, Amsterdam, Developments in Sedimentology Series, v. 58, p. 517-545.
- Garzanti, E., Andò, S., and Vezzoli, G., 2009, Grain-size dependence of sediment composition and environmental bias in provenance studies: Earth and Planetary Science Letters, v. 277, p. 422-432.
- Garzanti, E., Vezzoli, G., Andò, S., France-Lanord, C., Singh, S. K., and Foster, G., 2004, Sand petrology and focused erosion in collision orogens: the Brahmaputra case: Earth and Planetary Science Letters, v. 220, no. 1–2, p. 157-174.
- Ghosh, P., Padia, J. T., and Mohindra, R., 2004, Stable isotopic studies of palaeosol sediment from Upper Siwalik of Himachal Himalaya: evidence for high monsoonal intensity during late Miocene?: Palaeogeography, Palaeoclimatology, Palaeoecology, v. 206, no. 1–2, p. 103-114.
- Hébert, R., Bezard, R., Guilmette, C., Dostal, J., Wang, C. S., and Liu, Z. F., 2012, The Indus–Yarlung Zangbo ophiolites from Nanga Parbat to Namche Barwa syntaxes, southern Tibet: First synthesis of petrology, geochemistry, and geochronology with incidences on geodynamic reconstructions of Neo-Tethys: Gondwana Research, v. 22, no. 2, p. 377-397.
- Hillier, S., 1995, Erosion, Sedimentation and Sedimentary Origin of Clays, in Velde, B., ed., Origin and

Mineralogy of Clays: Clays and the Environment: Berlin, Heidelberg, Springer Berlin Heidelberg, p. 162-219.

- Hodges, K. V., 2000, Tectonics of the Himalaya and southern Tibet from two perspectives: Geological Society of America Bulletin, v. 112, no. 3, p. 324-350.
- Holtzappel, T., 1985, Les minéraux argileux, préparation, analyse diffractométrique et détermination.: Soc. Géol.Nord., v. 12, p. 1-36.
- Hu, X., Wang, J., BouDagher-Fadel, M., Garzanti, E., and An, W., 2016, New insights into the timing of the India–Asia collision from the Paleogene Quxia and Jialazi formations of the Xigaze forearc basin, South Tibet: Gondwana Research, v. 32, p. 76-92.
- Hubert, J. F., 1962, A zircon-tourmaline-rutile maturity index and the interdependence of the composition of heavy minerals assemblages with the gross composition and texture of sandstones: Journal of Sedimentary Petrology v. 32, p. 440-450.
- Huyghe, P., Guilbaud, R., Bernet, M., Galy, A., and Gajurel, A. P., 2011, Significance of the clay mineral distribution in fluvial sediments of the Neogene to Recent Himalayan Foreland Basin (west-central Nepal): Basin Research, v. 23, no. 3, p. 332-345.
- Huyghe, P., Mugnier, J.-L., Gajurel, A. P., and Delcaillau, B., 2005, Tectonic and climatic control of the changes in sedimentary record of the Karnali River section (Siwaliks of western Nepal). The Island Arc, v. 14, p. 311-327.
- Huyghe, P., Galy, A., Mugnier, J.-L., and France-Lanord, C., 2001, Propagation of the thrust system and erosion in the Lesser Himalaya: Geochemical and sedimentological evidences. Geology, v. 29, p. 1007–10.
- Ingersoll, R. V., Bullard, T. F., Ford, R. L., Grimm, J. P., Pickle, J. D., and Sares, S. W., 1984, The effect of grain size on detrital modes: a test of the Gazzi-Dickinson point-counting method.: Journal of Sedimentary Petrology, v. 54, p. 103-116.
- Karunakaran, C., and Rao, R. A., 1976, Status of Exploration of Hydrocarbon in the Himalayan Region-Contributions to Stratigraphy and Structure: Geological Society of India, Miscellaneous Publication, v. 41, p. 66 p.
- Kübler, B., and Goy-Eggenberger, D., 2001, La cristallinité de l'illite revisitée: Un bilan des connaissances acquises ces trente dernières années. : Clay Minerals, v. 36, p. 143-157.
- Kübler, B., and Jaboyedoff, M., 2000, Illite crystallinity: Comptes Rendus de l'Académie des Sciences -Series IIA - Earth and Planetary Science, v. 331, no. 2, p. 75-89.
- Kumar, G., 1997, Geology of Arunachal Pradesh: Bangalore: Geological Society of India, p. 217.
- Lanson, B., Beaufort, D., Berger, G., Baradat, J., and Lacharpargne, J.-C., 1996. Illitization of diagenetic kaolinite-to-dickite conversion series; late-stage diagenesis of the Lower Permian Rotliegend Sandstone reservoir, offshore of the Netherlands: Journal of Sedimentary Research, v. 66, p. 501-518.
- Le Fort, P., 1986, Metamorphism and magmatism during the Himalayan collision: Geological Society, London, Special Publications, v. 19, no. 1, p. 159-172.
- Lupker, M., France-Lanord, C., Galy, V., Lavé, J., Gaillardet, J., Gajurel, A. P., Guilmette, C., Rahman, M., Singh, S. K., and Sinha, R., 2012, Predominant floodplain over mountain weathering of Himalayan sediments (Ganga basin): Geochimica et Cosmochimica Acta, v. 84, p. 410-432.
- Lupker, M., France-Lanord, C., Galy, V., Lavé, J., and Kudrass, H., 2013, Increasing chemical weathering in the Himalayan system since the Last Glacial Maximum: Earth and Planetary Science Letters, v. 365, no. 0, p. 243-252.
- Mange, M. A., and Maurer, H. F. W., 1992, Heavy minerals in colour.: Chapman and Hall, London, p. 147 pp.
- Molnar, P., England, P., and Martinod, J., 1993, Mantle dynamics, uplift of the Tibetan Plateau, and the Indian Monsoon: Reviews of Geophysics, v. 31, no. 4, p. 357-396.
- Moore, D. M., and Reynolds, R. C., 1997, X-Ray diffraction and the identification and analysis of clay minerals, Oxford University Press.

Najman, Y., Appel, E., Boudagher-Fadel, M., Bown, P., Carter, A., Garzanti, E., Godin, L., Han, J.,

Liebke, U., Oliver, G., Parrish, R., and Vezzoli, G., 2010, Timing of India-Asia collision: Geological, biostratigraphic, and palaeomagnetic constraints: Journal of Geophysical Research: Solid Earth, v. 115, no. B12.

- Nakayama, K., and Ulak, P. D., 1999, Evolution of fluvial style in the Siwalik Group in the foothills of the Nepal Himalaya: Sedimentary Geology, v. 125, no. 3–4, p. 205-224.
- Nesbitt, H.W., and Young, G.M., 1982, Early Proterozoic climates and plate motions inferred from major element chemistry of lutite: Nature, v. 299, p. 715–717.
- Ojha, T. P., Butler, R. F., DeCelles, P. G., and Quade, J., 2009, Magnetic polarity stratigraphy of the Neogene foreland basin deposits of Nepal: Basin Research, v. 21, no. 1, p. 61-90.
- Parker, A., 1970. An index of weathering for silicate rocks: Geological Magazine, v. 107, p. 501–504.
- Quade, J., and Cerling, T. E., 1995, Expansion of C4 grasses in the Late Miocene of Northern Pakistan: evidence from stable isotopes in paleosols: Palaeogeography, Palaeoclimatology, Palaeoecology, v. 115, no. 1–4, p. 91-116.
- Raymo, M. E., and Ruddiman, W. F., 1992, Tectonic forcing of late Cenozoic climate: Nature, v. 359, no. 6391, p. 117-122.
- Robinson, D. M., DeCelles, P. G., Garzione, C. N., Pearson, O. N., Harrison, T. M., and Catlos, E. J., 2003, Kinematic model for the Main Central thrust in Nepal: Geology, v. 31, no. 4, p. 359-362.
- Sanyal, P., Bhattacharya, S. K., Kumar, R., Ghosh, S. K., and Sangode, S. J., 2004, Mio–Pliocene monsoonal record from Himalayan foreland basin (Indian Siwalik) and its relation to vegetational change: Palaeogeography, Palaeoclimatology, Palaeoecology, v. 205, no. 1–2, p. 23-41.
- Sanyal, P., Sarkar, A., Bhattacharya, S. K., Kumar, R., Ghosh, S. K., and Agrawal, S., 2010, Intensification of monsoon, microclimate and asynchronous C4 appearance: Isotopic evidence from the Indian Siwalik sediments: Palaeogeography, Palaeoclimatology, Palaeoecology, v. 296, no. 1–2, p. 165-173.
- Singh, S. K., and France-Lanord, C., 2002, Tracing the distribution of erosion in the Brahmaputra watershed from isotopic compositions of stream sediments: Earth and Planetary Science Letters, v. 202, no. 3–4, p. 645-662.
- Tagami, T. and O'Sullivan, P.B., 2005, Fundamentals of fission-track thermochronology: Reviews in Mineralogy and Geochemistry, v. 58, p. 19-47.
- Thiede, R. C., Bookhagen, B., Arrowsmith, J. R., Sobel, E. R., and Strecker, M. R., 2004, Climatic control on rapid exhumation along the Southern Himalayan Front: Earth and Planetary Science Letters, v. 222, no. 3–4, p. 791-806.
- van der Beek, P., Robert, X., Mugnier, J.-L., Bernet, M., Huyghe, P., and Labrin, E., 2006, Late Miocene – Recent exhumation of the central Himalaya and recycling in the foreland basin assessed by apatite fission-track thermochronology of Siwalik sediments, Nepal: Basin Research, v. 18, no. 4, p. 413-434.
- Vögeli, N., Najman, Y., van der Beek, P., Huyghe, P., and Wynn, P., 2015, Climatic variation along strike in the Himalayas since Mid-Miocene: AGU Abstract.
- Warr L.N., Rice H.N., 1994, Interlaboratory standardization and calibration of clay mineral crystallinity and crystallite size data: Journal of Metamorphic Geology, v. 12, p. 141–152.
- Wen, D.-R., Liu, D., Chung, S.-L., Chu, M.-F., Ji, J., Zhang, Q., Song, B., Lee, T.-Y., Yeh, M.-W., and Lo, C.-H., 2008, Zircon SHRIMP U–Pb ages of the Gangdese Batholith and implications for Neotethyan subduction in southern Tibet: Chemical Geology, v. 252, no. 3–4, p. 191-201.
- Yin, A., 2006, Cenozoic tectonic evolution of the Himalayan orogen as constrained by along-strike variation of structural geometry, exhumation history, and foreland sedimentation: Earth-Science Reviews, v. 76, no. 1–2, p. 1-131.
- Yin, A., Dubey, C. S., Kelty, T. K., Gehrels, G. E., Chou, C. Y., Grove, M., and Lovera, O. M., 2006, Structural evolution of the Arunachal Himalaya and implications for asymmetric development of the Himalayan orogen: Current Science, v. 90, no. 2, p. 195-206.

Yin, A., and Harrison, T. M., 2000, Geologic Evolution of the Himalayan-Tibetan Orogen: Annual Review of Earth & Planetary Sciences, v. 28, no. 1, p. 211.

Figures

Figure 1: Geological map of the Eastern Himalaya, modified from Chirouze et al. (2013). Red star indicates the Siwalik Section along the Kameng River. Red circles indicate sampling locations of modern river sand and mud. page 3.

Figure 2: Summary of heavy mineral and petrography data of the Kameng river section. page 4.

Figure 3: Changes in the composition of Siwalik sandstones in the last 13 Ma are controlled by both provenance and diagenesis. Strongly diagenized sandstones in the hanging wall of the Tippi thrust (TT) are richer in quartz and yield heavy-mineral assemblages dominated by relatively stable garnet, zircon and tourmaline (in brown). Litho-feldspatho-quartzose sandstones younger than 8 Ma (in green) in the footwall of the Tippi thrust are less diagenized and display compositions compatible with both modern Kameng sand (this study) and Brahmaputra sand collected at Tezpur (data from Garzanti et al., 2004). Detrital modes that are very different from modern Kameng are depicted in blue. These include sample KM13-5 from within the Tippi Thrust (13 Ma), sample KM13-2 (8.3 Ma) from the base of the footwall succession, and sample KM13-19 (2 Ma), which is quartzose with only few stable heavy minerals, suggesting deposition by a tributary largely recycling LHS quartzites. Q = quartz; F = feldspar; L = lithic grains (Lvm = volcanic, low-rank metavolcanic and high-rank felsic metamorphic; ZTR = zircon + tourmaline + rutile; CSKA = chloritoid + staurolite + kyanite + andalusite + sillimanite). page 8.

Figure 4: ZTR index (sum of zircon, tourmaline and rutile over total transparent heavy minerals; Hubert, 1962), abundance of garnet [%] and total heavy minerals [%] vs age [Ma] and stratigraphic depth [m]. The ZTR index generally increases with age/depth, indicating more dissolution with increasing stratigraphic burial. Garnet shows relative enrichment with increasing depth. Heavy mineral abundance decreases with depth. The sample at 13 Ma (grey band) is anomalous and appears to be influenced by the Tippi Thrust. page 8.

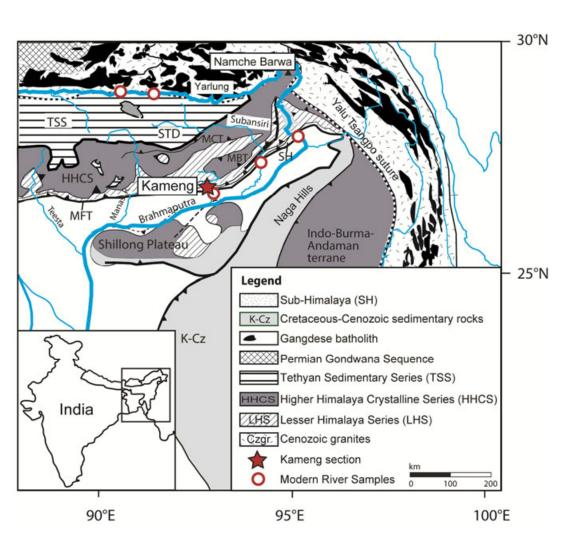
Figure 5: Illite+Chlorite/Sum of clays and illite crystallinity [$\Delta^{\circ}2\theta$] on ethylen-glycol (EG – full symbols) and air-dried scans (AD – open symbols) vs age [Ma] and depth [m]. Triangles indicate modern river samples, grey circles show samples with anomalous clay assemblages. Provenance, as determined from Nd and Hf isotopes (Chirouze et al., 2013) and from detrital zircon U-Pb ages (Cina et al., 2009), is indicated on the right. The grey star indicates the illite crystallinity of a clay sample from a small stream within the Higher Himalaya Crystalline Sequence (Huyghe et al., 2011). No clear trend in illite crystallinity is observed with depth. page 9.

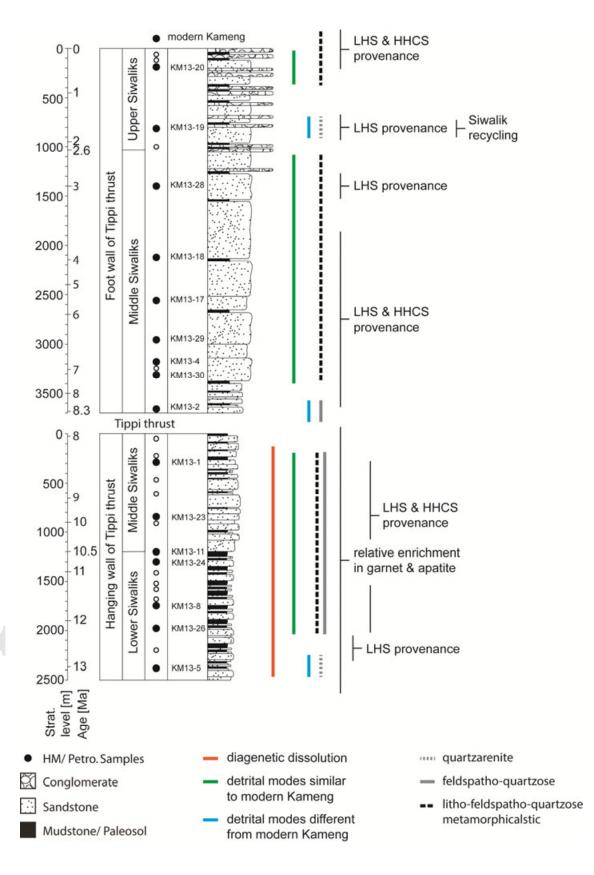
Figure 6: Clay mineral assemblages of modern rivers (1,2: Yarlung, 3: Siang, 4: Subansiri, 5: Kameng) in the Eastern Himalaya. Geological base map modified after Chirouze et al. (2013). page 9.

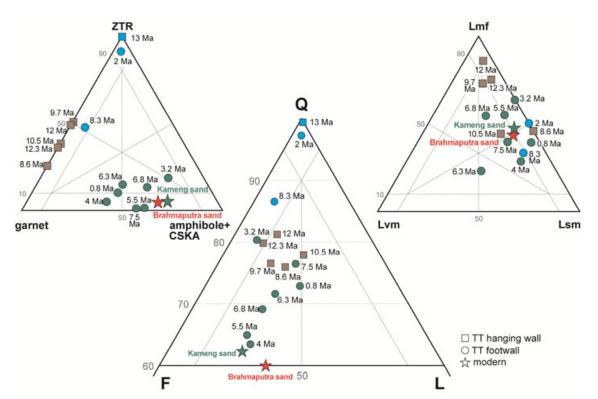
Figure 7: Correlation between SiO₂ and K_2O , Al_2O_3 and H_2O^+ , fine-grained sediments (in black) show depletion in SiO₂. Mineralogy and major element concentrations vary from fine- to coarse-grained sediments. page 10.

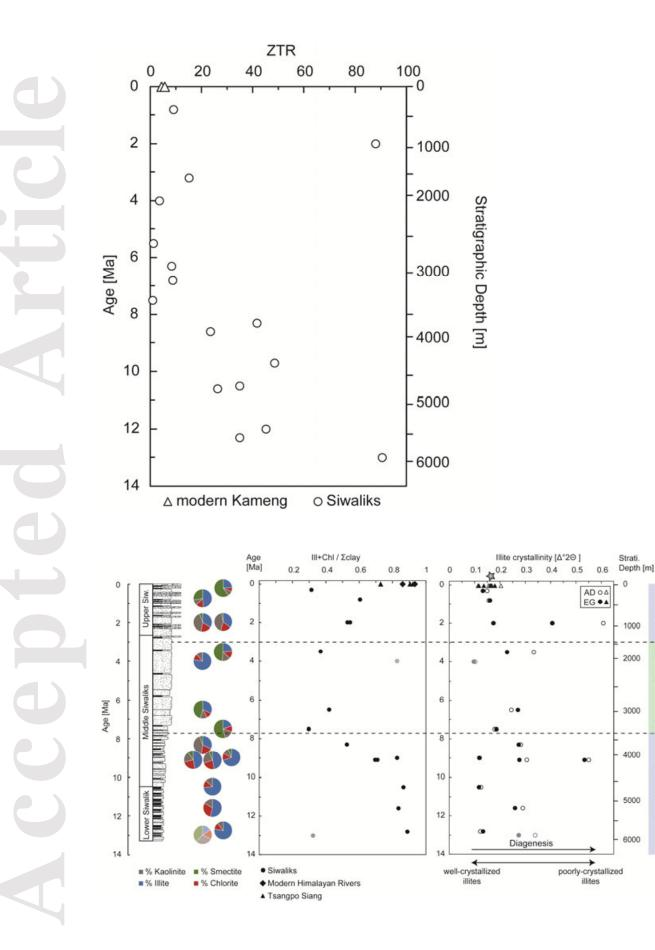
Figure 8: Evolution of K/Si vs. Al/Si of fine-grained (full circles) and coarse-grained (empty circles) Siwalik sediments of the Kameng section. Outliers are rocks sampled in proximity to the Tippi Thrust, for which we interpret the signal to be overprinted by dissolution due to fluid circulation. Different colors indicate different time periods (Lower Siwaliks – 13-10.5 Ma: red; Middle Siwaliks – 10.5-2.6 Ma: green; Upper Siwaliks - <2.6 Ma: yellow). Modern river samples from Lupker et al. (2013) are plotted in black (Himalayan tributatires) and grey (Brhmaputra main stem) diamonds. Best-fit regression lines through the LS, MS and US datasets are indicated as solid lines; dotted lines represent the 0.95 confidence level of the linear regression of the different time periods, in order to assess the significance of the inferred changes in weathering intensity over time. page 10.

Figure 9: Evolution of K/Si^{*}, H2O+/Si^{*} and K/Al over time in the Kameng River section. Arrows indicate a change in weathering regime. H_2O^+/Si^* is anti-correlated to K/Si^{*} and K/Al. Modern river values are indicated in grey/black diamonds. Outliers are encircled and show sediments influenced by fluid flow in the Tippi Thrust. page 10.







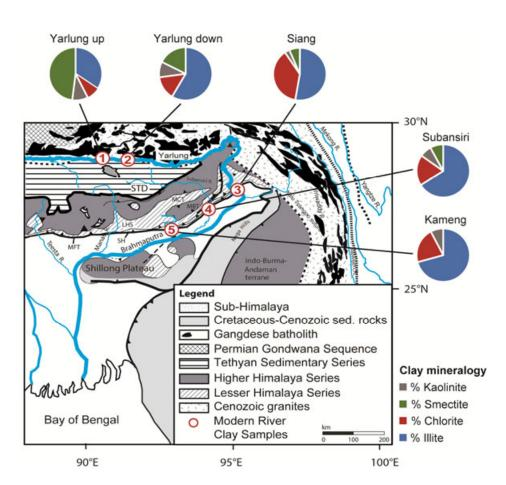


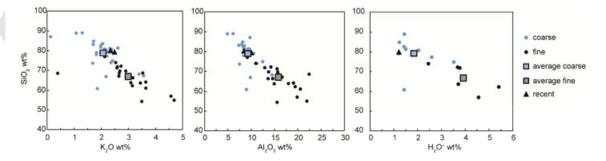
HHCS & LHS

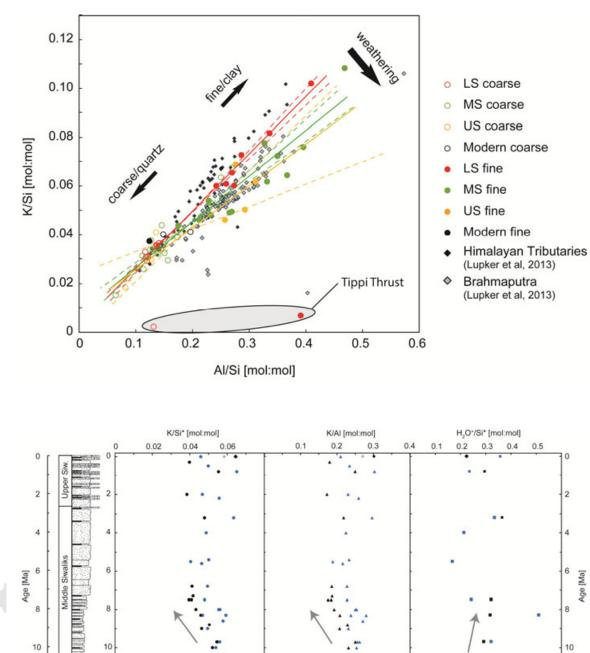
Batholith

Gangdese

HHCS & LHS







Tippi Thrust

weathering

[Ma]

Age

12

14

weathering

>+

This article is protected by copyright. All rights reserved.

weathering

Siwalik

OWPL

• • • coarse

• • • fine · · modern (coarse/fine)

12

14

lippi hrust

12

14